

Chapter 6

Alternatives to DAS

Throughout the preceding chapters both the theory and recent experimental advances of dynamic-angle spinning NMR have been discussed. This experiment was developed to produce high-resolution liquid-like spectra from solid samples containing quadrupolar nuclei such as ^{17}O , ^{23}Na and ^{27}Al . Other techniques for averaging both the quadrupolar and chemical shift interactions have also been developed, including double rotation^{55,108}, magic-angle hopping^{109,110}, magic-angle turning¹¹¹ and dynamic-angle hopping.⁵⁶

Double Rotation (DOR)

Double rotation is the simultaneous solution to the quadrupolar spinning problem in which at least two angles are required to give narrow isotropic spectra.⁵⁵

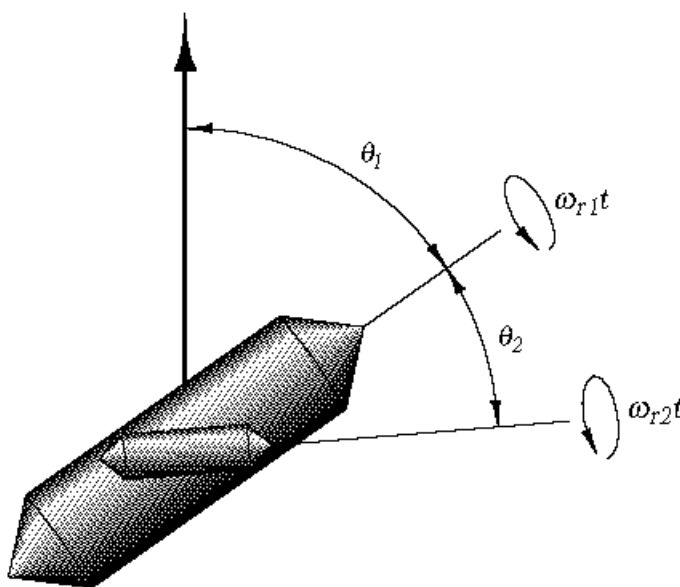


Figure 6.1 DOR Rotor & Rotations. A representation of a DOR rotor is shown with the rotation angles given. These correspond to those shown in equation 6.1. The phase of the outer rotor is defined to be zero at zero time when the inner rotor makes the smallest angle with respect to the vertical axis (the magnetic field).

In this experiment, a small rotor is spun about an axis which slowly moves in a conical fashion about the magic-angle with respect to the magnetic field. Figure 6.1 shows the

rotations needed to go from the PAS frame to the inner rotor frame then to the outer rotor frame and finally to the laboratory frame. The expression for the frequency under this time dependent trajectory is given below in equation 6.1.

$$\Delta E^{(2Q)} = \frac{\hbar 2\omega_Q^2}{\omega_I} \left(I(I+1) - \frac{3}{4} \right) \frac{\langle l, 0 | 2, 2, m, -m \rangle}{m} a_{l0}^Q$$

$$a_{l0}^Q = \prod_{n=-l}^l D_{n0}^{(l)}(\omega_{r1}t + \phi_{r1}, \theta_1, 0) \prod_{j=-l}^l D_{jn}^{(l)}(\omega_{r2}t + \phi_{r2}, \theta_2, 0)$$

$$\times \prod_{k=-l}^l D_{kj}^{(l)}(\alpha^Q, \beta^Q, \gamma^Q) \sigma_{lk}^Q \quad (6.1)$$

In this expression, θ_1 is the angle the outer rotation axis makes with respect to the magnetic field and θ_2 is the angle the inner rotation axis makes with respect to the outer rotation axis. The outer rotation rate and absolute rotor phase are given by ω_{r1} and ϕ_1 while the inner rotation rate and absolute rotor phase are given by ω_{r2} and ϕ_2 . The outer rotor phase is defined as zero when the inner rotation axis makes the smallest angle with respect to the magnetic field. The Euler angles refer to the rotation from the PAS to the inner rotor reference frames. Under the assumption of high speed spinning about both axes, this expression is greatly simplified.

$$\Delta E^{(2Q)} = \frac{\hbar 2\omega_Q^2}{\omega_I} \left(I(I+1) - \frac{3}{4} \right) \frac{\langle l, 0 | 2, 2, m, -m \rangle}{m} a_{l0}^Q$$

$$a_{l0}^Q = d_{00}^{(l)}(\theta_1) d_{00}^{(l)}(\theta_2) \prod_{k=-l}^l e^{-ik\alpha^Q} D_{k0}^{(l)}(\beta^Q) \sigma_{lk}^Q \quad (6.2)$$

Much like the case of high speed magic angle spinning, the appearance of terms proportional to Legendre polynomials leads to the choice of DOR spinning angles. In the above expression, if θ_2 is chosen equal to the root of the fourth-order Legendre polynomial $P_4[\cos\theta_2]$ and θ_1 is chosen equal to the root of the second-order Legendre polynomial

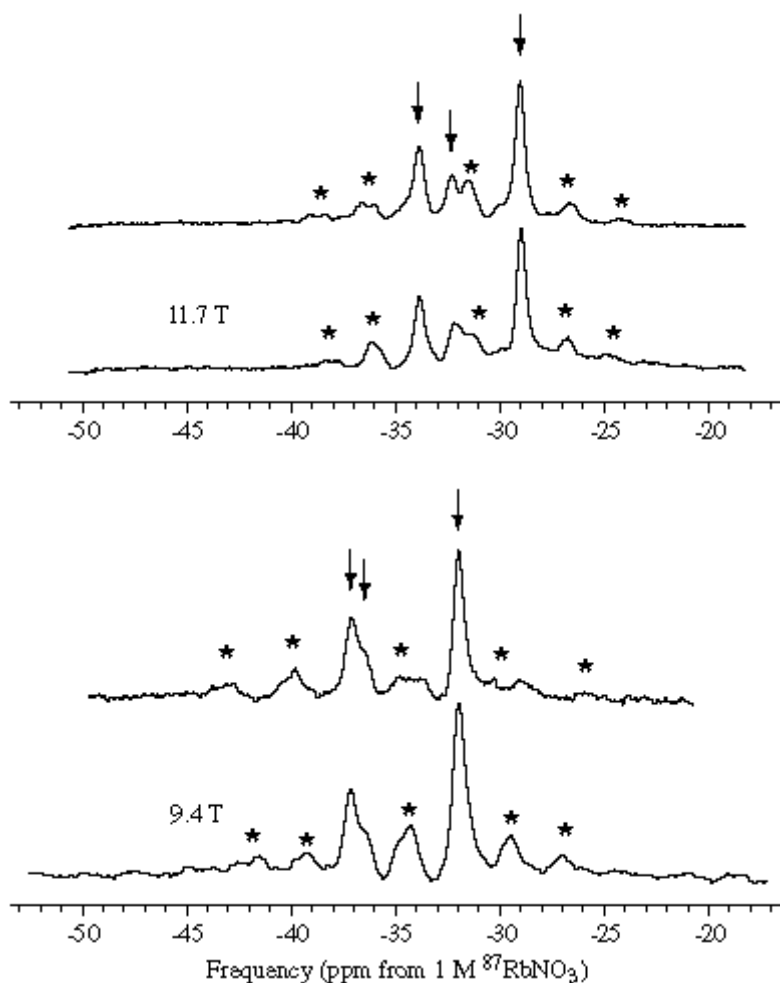


Figure 6.2 DOR of $^{87}\text{RbNO}_3$ at 9.4T. The two spectra above were taken with short 30° pulses and a rapid repetition rate. This allowed acquisition of a large number of scans with random rotor phases, to achieve complete averaging of this variable leading to all positive sideband amplitudes (see below). The Larmor frequency at 11.7T was 163.628 MHz and 130.886 MHz at 9.4T. The spinning rates were 500 Hz (lower spectrum of each pair) and 700 Hz (upper spectrum) in these experiments.

$P_2[\cos\theta_1]$, only the $l = 0$ terms will be non-zero. Alternatively, the angles may be reversed with the same effect. There is only one angle which is the root of $P_2[\cos\theta_1]$ which is the magic angle, 54.74° , while two angles are the roots of $P_4[\cos\theta_2]$, 30.56°

and 70.12°. Due to the requirements of constructing a DOR probehead, the usual choice is 54.74° for the outer rotor and 30.56° for the inner rotor. With these angles chosen, the DOR experiment is a simple single pulse and acquire experiment. Figure 6.2 shows the DOR spectra for $^{87}\text{RbNO}_3$, a salt with three crystallographically distinct sites. The spinning sidebands (marked with asterisks) arises from the time dependent terms which were ignored in equation 6.2. The isotropic peaks (marked with vertical arrows) are those which do not change position when the spinning rate is changed. These correspond to peaks at -29, -32 and -34 ppm at 11.7T (163.628 MHz Larmor frequency) and -32, -36 and -37 at 9.4T (130.886 MHz Larmor frequency). The time dependent terms which lead to spinning sidebands may be analyzed in a manner virtually identical to that presented in chapter 3. First, we expand the energy splitting in equation 6.1 as the sum of oscillating time dependent terms.

$$\Delta E^{(2Q)} = \frac{\hbar 2\omega_Q^2}{\omega_I} \left(I(I+1) - \frac{3}{4} \right) \sum_{l=0,2,4} \sum_{m>0} \frac{\langle l,0|2,2,m,-m\rangle}{m} a_{l0}^Q$$

$$a_{l0}^Q = \sum_{n=-l}^l \sum_{j=-l}^l \sum_{k=-l}^l d_{jn}^{(l)}(\theta_2) d_{n0}^{(l)}(\theta_1) d_{kj}^{(l)}(\beta^Q) \sigma_{lk}^Q$$

$$\times e^{-i \left[n(\omega_{r1}t + \phi_{r1}) + j(\omega_{r2}t + \phi_{r2} + \gamma^Q) + k\alpha^Q \right]}$$
(6.3)

This expression may then be regrouped according to the dependence on rotation rates.

$$\Delta E^{(2Q)} = \sum_{l=0,2,4} \sum_{n,j=-l}^l W_{nj}^{(l)} e^{-i \left[n(\omega_{r1}t + \phi_{r1}) + j(\omega_{r2}t + \phi_{r2} + \gamma^Q) \right]}$$

$$W_{nj}^{(l)} = \frac{\hbar 2\omega_Q^2}{\omega_I} \left(I(I+1) - \frac{3}{4} \right) d_{jn}^{(l)}(\theta_2) d_{n0}^{(l)}(\theta_1) \sum_{k=-l}^l d_{kj}^{(l)}(\beta^Q) \sigma_{lk}^Q$$

$$\times e^{-ik\alpha^Q} \sum_{m>0} \frac{\langle l,0|2,2,m,-m\rangle}{m}$$
(6.4)

This may then be simplified by grouping the $l = 0, 2,$ and 4 terms together for each n, j pair. This simplifies equation 6.4 even further.

$$\Delta E^{(2Q)} = \sum_{n,j=-4}^4 W_{nj} e^{-i[n(\omega_{r1}t + \phi_{r1}) + j(\omega_{r2}t + \phi_{r2} + \gamma \varrho)]} \quad (6.5)$$

$$W_{nj} = \sum_{l=0,2,4} W_{nj}^{(l)}$$

This may then be integrated to give the evolved phase and signal after a 90° pulse.

$$\phi^{DOR}(t) = W_{00}t + \sum_{\substack{n,j=-4 \\ j=n \ 0}}^4 \frac{W_{nj} e^{-i[n(\omega_{r1}t + \phi_{r1}) + j(\omega_{r2}t + \phi_{r2} + \gamma \varrho)]}}{-i(n\omega_{r1} + j\omega_{r2})} \quad (6.6a)$$

$$+ \sum_{\substack{n,j=-4 \\ j=n \ 0}}^4 \frac{-W_{nj} e^{-i[n\phi_{r1} + j(\phi_{r2} + \gamma \varrho)]}}{-i(n\omega_{r1} + j\omega_{r2})}$$

$$S(t) = e^{-i\phi^{DOR}(t)} = e^{-iW_{00}t} \times \exp \sum_{\substack{n,j=-4 \\ j=n \ 0}}^4 \frac{W_{nj} e^{-i[n(\omega_{r1}t + \phi_{r1}) + j(\omega_{r2}t + \phi_{r2} + \gamma \varrho)]}}{(n\omega_{r1} + j\omega_{r2})} \quad (6.6b)$$

$$\times \exp \sum_{\substack{n,j=-4 \\ j=n \ 0}}^4 \frac{-W_{nj} e^{-i[n\phi_{r1} + j(\phi_{r2} + \gamma \varrho)]}}{(n\omega_{r1} + j\omega_{r2})}$$

The use of Dirac delta functions again may be used to simplify this equation.

$$S(t) = e^{-iW_{00}t} \int_0^{2\pi} \int_0^{2\pi} \delta(\psi - \omega_{r1}t - \phi_{r1}) \delta(\psi - \omega_{r2}t - \phi_{r2} - \gamma \varrho) \times \frac{1}{4\pi^2} \times \exp \sum_{\substack{n,j=-4 \\ j=n \ 0}}^4 \frac{W_{nj} e^{-i[n\psi + j\psi]}}{(n\omega_{r1} + j\omega_{r2})} d\psi d\psi \quad (6.7)$$

$$\int_0^{2\pi} \int_0^{2\pi} \delta(\psi - \phi_{r1}) \delta(\psi - \phi_{r2} - \gamma \varrho) \times \frac{1}{4\pi^2} \times \exp \sum_{\substack{n,j=-4 \\ j=n \ 0}}^4 \frac{-W_{nj} e^{-i[n\psi + j\psi]}}{(n\omega_{r1} + j\omega_{r2})} d\psi d\psi$$

Then substituting back the infinite sum expansion for the Dirac delta functions gives equation 6.8.

$$\begin{aligned}
S(t) = e^{-iW_{00}t} & \times \frac{1}{4\pi^2} \int_{N_1, N_2} \int_0^{2\pi} \int_0^{2\pi} \exp \left[iN_1(\psi - \omega_{r1}t - \phi_{r1}) + \sum_{\substack{n,j=-4 \\ j=n}}^4 \frac{W_{nj} e^{-i[n\psi + j\psi]}}{(n\omega_{r1} + j\omega_{r2})} \right] d\psi d\psi \\
& + iN_2(\psi - \omega_{r2}t - \phi_{r2} - \gamma \varrho) \\
& \times \frac{1}{4\pi^2} \int_{N_3, N_4} \int_0^{2\pi} \int_0^{2\pi} \exp \left[iN_3(\psi - \phi_{r1}) + \sum_{\substack{n,j=-4 \\ j=n}}^4 \frac{-W_{nj} e^{-i[m\psi + j\psi]}}{(n\omega_{r1} + j\omega_{r2})} \right] d\psi d\psi \\
& + iN_4(\psi - \phi_{r2} - \gamma \varrho)
\end{aligned} \tag{6.8}$$

The ψ and ψ' independent terms may be removed from the integrals and the signal may be expressed below.

$$\begin{aligned}
S(t) = e^{-iW_{00}t} & A_{N_1, N_2} A_{N_3, N_4}^* e^{-i[N_1\omega_{r1} + N_2\omega_{r2}]t} \\
& \times e^{-i[(N_1 - N_3)\phi_{r1} + (N_2 - N_4)(\phi_{r2} + \gamma \varrho)]} \\
A_{N_1, N_2} = \frac{1}{4\pi^2} & \int_0^{2\pi} \int_0^{2\pi} \exp \left[iN_1\psi + iN_2\psi + \sum_{\substack{n,j=-4 \\ j=n}}^4 \frac{W_{nj} e^{-i[m\psi + j\psi]}}{(n\omega_{r1} + j\omega_{r2})} \right] d\psi d\psi
\end{aligned} \tag{6.9}$$

This expression may then be integrated over the inner rotor phase ($N_2 = N_4$) due to the fact that usually we observe signal from powder samples (all $\gamma \varrho$ will be present).

$$\langle S(t) \rangle_{\phi_{r2} + \gamma \varrho} = e^{-iW_{00}t} \int_{N_1, N_2, N_3} A_{N_1, N_2} A_{N_3, N_2}^* e^{-i[N_1\omega_{r1} + N_2\omega_{r2}]t} e^{-i[(N_1 - N_3)\phi_{r1}]} \tag{6.10}$$

The signal may then be averaged over all the powder angles and outer rotor orientations.

$$\begin{aligned}
\langle S(t) \rangle_{\text{powder}} & = e^{-i\omega_{iso}^{(2Q)}t} S_{N_1, N_2} e^{-i[N_1\omega_{r1} + N_2\omega_{r2}]t} \\
S_{N_1, N_2} & = \frac{1}{4\pi} \int_0^{2\pi} \int_0^\pi |A_{N_1, N_2}|^2 \sin\beta \varrho d\beta \varrho d\alpha \varrho
\end{aligned} \tag{6.11}$$

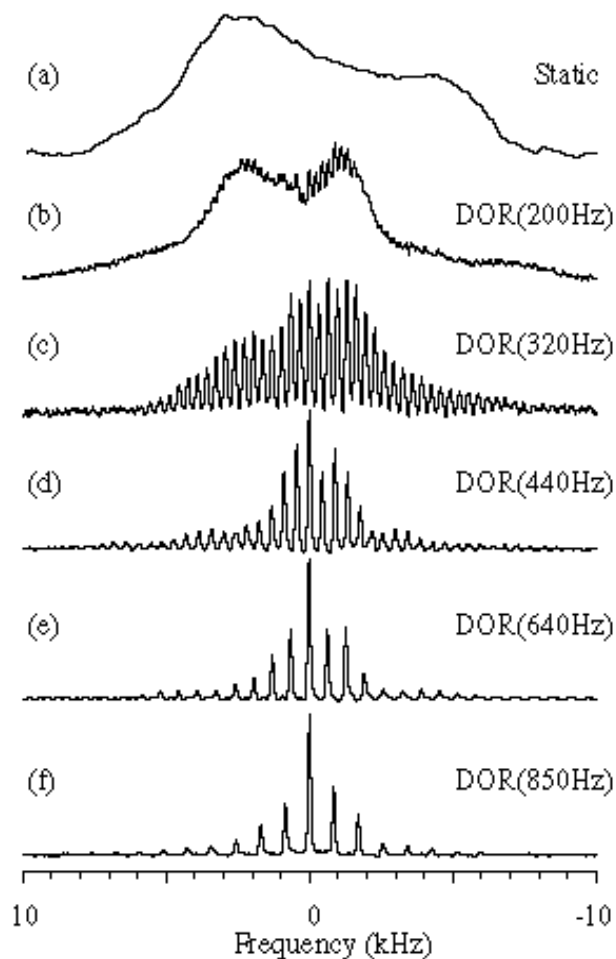


Figure 6.3 DOR of $^{23}\text{Na}_2\text{C}_2\text{O}_4$ at 9.4T. The spectra above were taken with the usual short pulses and a rapid repetition rate. Shown are the sideband intensities and positions for a variety of spinning rates (outer rotor spinning rate indicated beside each spectrum). It is important to note that the intensities do not necessarily approximate the powder pattern in the slow spinning limit.

This shows that spinning sidebands will show up at sums and differences of integers times the rotor frequencies. In general, the strongest sidebands will be those with small N_1 and N_2 values. For a more detailed analysis of DOR spinning sideband intensities, see papers by Sun *et al.*^{16,49} In figure 6.3 are shown the experimental DOR spectra of sodium oxalate at a variety of spinning rates. The most important feature here is that even in the slow spinning limit, the sideband intensities do not approximate the shape of the static pattern, as occurs in spin 1/2 systems under MAS. The spectra in figure 6.3 were taken by B.Q. Sun and Y. Wu and details concerning their acquisition may be found in their papers.^{16,49,112}

In addition, certain symmetry considerations can lead to the cancellation of all of the odd-order outer frequency sidebands leading to greater sensitivity and resolution.^{49,100,108,112-114} To show this effect, we return to equation 6.6 and assume that the inner rotor is spinning much faster than the outer rotor and average over this motion.

$$\begin{aligned} \phi^{DOR}(t) &= W_{00}t + \sum_{n=0} \frac{W_{n0} \left(e^{-in(\omega_{r1}t + \phi_{r1})} - e^{-in\phi_{r1}} \right)}{-in\omega_{r1}} \\ S(t) &= e^{-iW_{00}t} \exp \sum_{n=0} \frac{W_{n0} \left(e^{-in(\omega_{r1}t + \phi_{r1})} - e^{-in\phi_{r1}} \right)}{n\omega_{r1}} \end{aligned} \quad (6.12)$$

This, of course, now looks similar to the expression for the VAS signal in equation 3.11 or 3.21. There is one major difference, in that now the following substitution may be made for $W_{-n0} = -W_{n0}$. In fact, were this true for the VAS case, it would be possible to eliminate all odd order sidebands from any one dimensional experiment. This is not the case, however, and the rotor-synchronized acquisition described below will only give its effective speed enhancement under DOR conditions.

$$S(t) = e^{-iW_{00}t} \exp \sum_{n>0} \frac{W_{n0} \left(\cos n(\omega_{r1}t + \phi_{r1}) - \cos n\phi_{r1} \right)}{n\omega_{r1}} \quad (6.13)$$

Signal may now be collected through outer-rotor synchronization such that the outer rotor phase is only 0° or 180° . When this is done, the signal may be written below.

$$\begin{aligned} \langle S(t) \rangle^{0^\circ+180^\circ} &= e^{-iW_{00}t} \exp \sum_{n=2,4} \frac{W_{n0} \left(\cos n\omega_{r1}t - 1 \right)}{n\omega_{r1}} \\ &= e^{-iW_{00}t} \exp \sum_{n=1,2} \frac{W_{2n0} \left(\cos n\omega_{r3}t - 1 \right)}{n\omega_{r3}} \\ \omega_{r3} &= 2\omega_{r1} \end{aligned} \quad (6.14)$$

Notice that a redefinition of the spinning rate has been made which changes the indices of the sum. This may be expanded with delta functions as before.

$$\begin{aligned} \langle S(t) \rangle^{0^\circ+180^\circ} &= e^{-iW_{00}t} \exp \sum_{n=1,2} \frac{-W_{2n0}}{n\omega_{r3}} \\ &\times \frac{1}{2\pi} \int_0^{2\pi} \delta(\psi - \omega_{r3}t) \exp \sum_{n=1,2} \frac{W_{2n0} \cos n\psi}{n\omega_{r3}} d\psi \end{aligned} \quad (6.15)$$

Using the series expansion for a delta function we arrive at equation 6.16.

$$\begin{aligned} \langle S(t) \rangle^{0^\circ+180^\circ} &= e^{-iW_{00}t} \exp \sum_{n=1,2} \frac{-W_{2n0}}{n\omega_{r3}} \\ &\times \frac{1}{2\pi} \int_0^{2\pi} \exp iN(\psi - \omega_{r3}t) + \sum_{n=1,2} \frac{W_{2n0} \cos n\psi}{n\omega_{r3}} d\psi \end{aligned} \quad (6.16)$$

Now we pull out constant terms from the integrals, just as in equation 3.14.

$$\begin{aligned} \langle S(t) \rangle^{0^\circ+180^\circ} &= e^{-iW_{00}t} \exp \sum_{n=2,4} \frac{-W_{n0}}{n\omega_{r1}} A_N e^{-2iN\omega_{r1}t} \\ A_N &= \frac{1}{2\pi} \int_0^{2\pi} \exp iN\psi + \sum_{n=2,4} \frac{W_{n0} \cos(n\psi/2)}{n\omega_{r1}} d\psi \end{aligned} \quad (6.17)$$

This signal may then be averaged over the remaining powder angles, giving the result in equation 6.18.

$$\begin{aligned} \langle S(t) \rangle_{powder}^{0^\circ+180^\circ} &= \frac{1}{4\pi} e^{-i\omega_{iso}^{(2Q)}t} e^{-2iN\omega_{r1}t} \\ &\times \int_0^{2\pi} \int_0^\pi \exp \sum_{n=2,4} \frac{-W_{n0}}{n\omega_{r1}} A_N \sin \beta^Q d\beta^Q d\alpha^Q \end{aligned} \quad (6.18)$$

This expression shows immediately that the sidebands will be spaced at twice the outer rotor spinning speed from the isotropic peak. This is quite useful, since it is difficult to spin a DOR outer rotor much faster than 1 kHz and there will always be a large number of spinning sidebands present to complicate spectra. Figure 6.4 gives an example of the advantages of synchronized DOR when applied to the ^{23}Na spectrum of $\text{Na}_2\text{C}_2\text{O}_4$.

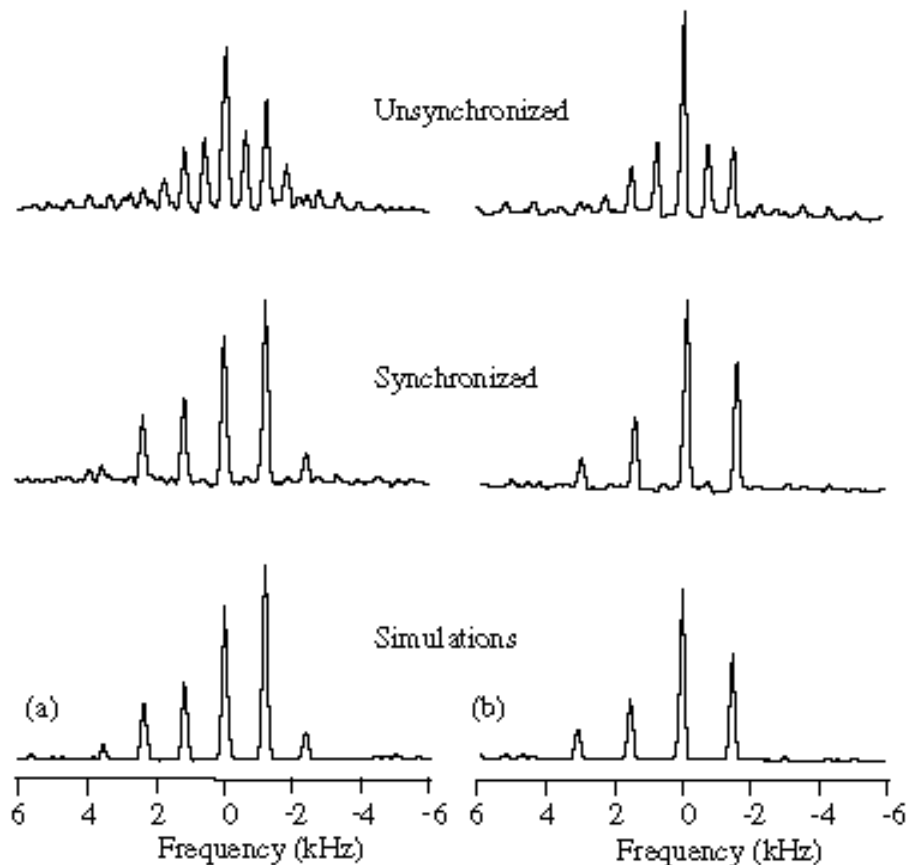


Figure 6.4 DOR of $^{23}\text{Na}_2\text{C}_2\text{O}_4$ at 9.4T. The spectra above were taken with short 30° pulses and a rapid repetition rate. Absolute rotor phase was monitored using optical methods and pulses were applied only at the 0° and 180° positions. The outer rotor spinning rate was 604 Hz for the spectra on the left and 800 Hz for those on the right. For the simulations, the parameters were $C_Q = 2.43$ MHz, $\eta_Q = 0.72$ and $\omega_I = 105.8$ MHz.

Magic-Angle Hopping (MAH)

A different kind of experiment which generates isotropic spectra for spin $1/2$ systems has been described by Bax *et al.*¹⁰⁹ In this experiment, a static sample is allowed to evolve at three different orientations which define the vertices of an octahedron. This is accomplished by using z-filters to store the evolved magnetization while the sample is rotated by 90 degrees about two orthogonal axes. The pulse sequence for this experiment is shown in figure 6.5.

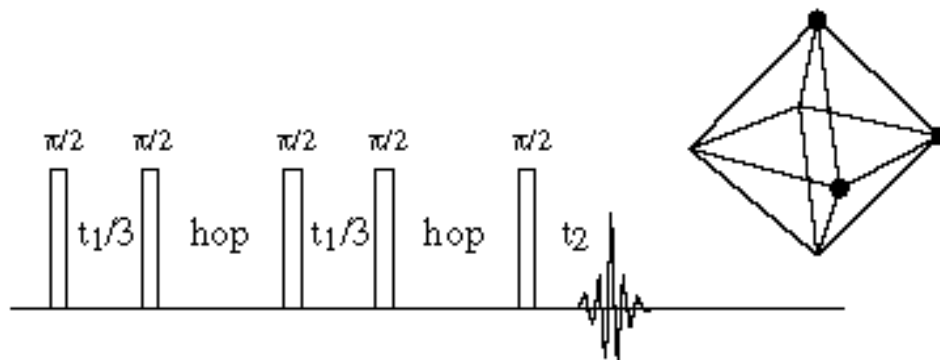


Figure 6.5 Magic-Angle Hopping Experiment. Pulses and hops are indicated schematically. The phase cycle is given in table 6.1. Each $t_{1/3}$ period is spent with the magnetic field pointing through each of three vertices of an octahedron attached to the PAS of a given crystallite.

Alternatively, MAH may be accomplished by rotating the sample about the magic angle in three discrete 120° jumps using the same pulse sequence. In any case, no spinning apparatus is required, however, the ability to perform rapid jumps may actually be of greater experimental complexity. Of these two implementations, the second is preferable, as it only requires rotation about a single axis.

ϕ_1	ϕ_2, ϕ_4, ϕ_5	ϕ_3	ϕ_r	ϕ_1	ϕ_2, ϕ_4, ϕ_5	ϕ_3	ϕ_r
0	0	0	0	180	0	180	0
0	0	90	90	180	0	270	90
0	0	180	180	180	0	0	180
0	0	270	270	180	0	90	270
90	0	270	0	270	0	90	0
90	0	0	90	270	0	180	90
90	0	90	180	270	0	270	180
90	0	180	270	270	0	0	270

Table 6.1 Magic-Angle Hopping Experimental Phase Cycle. Phase cycle for MAH where the phase ϕ_n refers to the n th pulse in the pulse sequence. This same phase cycle may also be used for the MAT experiment (see figure 6.6).

The phase cycle needed to implement this experiment is given in table 6.1. Both the first and third pulses are cycled through four phases each to select $\Delta p = -1$. The $\Delta p = +1$ will

be selected automatically without phase cycling the second or fourth pulses, since any non-zero coherences will decay during the hops. Finally, the last $\Delta p = -1$ will be selected by the quadrature phase of the receiver and merits no additional phase cycling, unless receiver quadrature is imperfect.

To show mathematically how the MAH evolution can generate an isotropic spectrum in the t_1 dimension of a two dimensional experiment we have to look at the frequency expression for the chemical shift interaction.

$$\begin{aligned}\omega_{CSA} &= \delta_{iso,cs}\omega_l + \sqrt{\frac{2}{3}}\delta^{CS}\omega_l A_{2,0}^{CS} \\ A_{2,0}^{CS} &= \sum_{m=-2}^2 D_{m,0}^{(2)}(\alpha^{CS}, \beta^{CS}, \gamma^{CS}) \rho_{2,m}^{CS}\end{aligned}\quad (6.19)$$

The three Euler angles relate the laboratory frame to the principal axis frame of reference. In an experiment where the sample is rotated α^{rot} about an axis oriented β^{rot} with respect to the magnetic field, this expression is modified as below.

$$\begin{aligned}\omega_{CSA} &= \delta_{iso,cs}\omega_l + \sqrt{\frac{2}{3}}\delta^{CS}\omega_l \sum_{m=-2}^2 D_{m,0}^{(2)}(\alpha^{rot}, \beta^{rot}, 0) A_{2,m}^{CS} \\ A_{2,m}^{CS} &= \sum_{m=-2}^2 D_{m,m}^{(2)}(\alpha^{CS}, \beta^{CS}, \gamma^{CS}) \rho_{2,m}^{CS}\end{aligned}\quad (6.20)$$

To examine the experiment where the sample is hopped in three 120 degree jumps about a given angle β^{rot} with respect to the magnetic field, we only have to sum up the evolution at each of the three rotor orientations. The three different orientations, expressed in the Euler angles are given below.

$$\begin{aligned}& (\alpha^{rot}, \beta^{rot}, 0) \\ (\alpha^{rot}, \beta^{rot}, 0) & \quad (\alpha^{rot} + \frac{2\pi}{3}, \beta^{rot}, 0) \\ & \quad (\alpha^{rot} + \frac{4\pi}{3}, \beta^{rot}, 0)\end{aligned}\quad (6.21)$$

The net evolved phase over a period t_1 may then be written below

$$\begin{aligned}
\phi^{MAH}(t_1) = & \delta_{iso,cs}\omega_l t_1 \\
& + \sqrt{\frac{2}{3}}\delta^{CS}\omega_l \frac{t_1}{3} \sum_{m=-2}^2 D_{m,0}^{(2)}(\alpha^{rot}, \beta^{rot}, 0) + A_{2,m}^{CS} D_{m,0}^{(2)}(\alpha^{rot} + \frac{2\pi}{3}, \beta^{rot}, 0) + A_{2,m}^{CS} D_{m,0}^{(2)}(\alpha^{rot} + \frac{4\pi}{3}, \beta^{rot}, 0)
\end{aligned} \tag{6.22}$$

The first term is the isotropic portion of the interaction which we wish to retain. The second is the anisotropic portion which will be shown to average to zero under the magic-angle hopping experiment. The first simplification comes by setting β^{rot} to the magic-angle (54.74°). This is the zero of the second-order Legendre polynomial and forces all of the $m = 0$ terms to be zero. Secondly, by separating the Wigner rotation matrices into products of exponentials and reduced Wigner matrices via equation 6.23, the sum in 6.22 may be further simplified.

$$D_{m,0}^{(2)}(\alpha^{rot}, \beta^{rot}, 0) = e^{-im\alpha^{rot}} d_{m,0}^{(2)}(\beta^{rot}) \tag{6.23}$$

In this expression, the $m = 0$ terms have been dropped as they are zero.

$$\begin{aligned}
\phi^{MAH}(t_1) = & \delta_{iso,cs}\omega_l t_1 + \sqrt{\frac{2}{3}}\delta^{CS}\omega_l \frac{t_1}{3} \sum_{m \neq 0} e^{-im\alpha^{rot}} d_{m,0}^{(2)}(\beta^{rot}) C_m A_{2,m}^{CS} \\
C_m = & 1 + e^{\frac{-2im\pi}{3}} + e^{\frac{-4im\pi}{3}}
\end{aligned} \tag{6.24}$$

The sum of exponentials (C_m) inside the sum over m is seen to be zero by using the following expressions.

$$\sum_{i=1}^n \cos \frac{2i\pi}{n} = \sum_{i=1}^n \sin \frac{2i\pi}{n} = 0 \quad \text{for } n > 1 \tag{6.25}$$

This effectively removes all of the anisotropic contribution to the evolution and the net evolution and signal are given below.

$$\begin{aligned}
\phi^{MAH}(t_1) = & \delta_{iso,cs}\omega_l t_1 \\
S(t_1) = & e^{-i\phi^{MAH}(t_1)} = e^{-i\delta_{iso,cs}\omega_l t_1}
\end{aligned} \tag{6.26}$$

An alternative approach to understanding this type of averaging scheme is to invoke group theoretical arguments as shown by Sun *et al.*^{16,113} This produces an identical result and will not be discussed here.

An excellent alternative to MAH is an experiment called magic-angle turning (MAT) first described by Gan.¹¹¹ In this experiment, the sample is rotated continuously about the magic-angle, just as in MAS. However, now the sample is rotated at a very slow spinning speed (less than 100 Hz). In this fashion, the evolution at each of the vertices of an octahedron may be approximated by interrupting the spinning with z-filters. This pulse sequence is seen in figure 6.6 below.

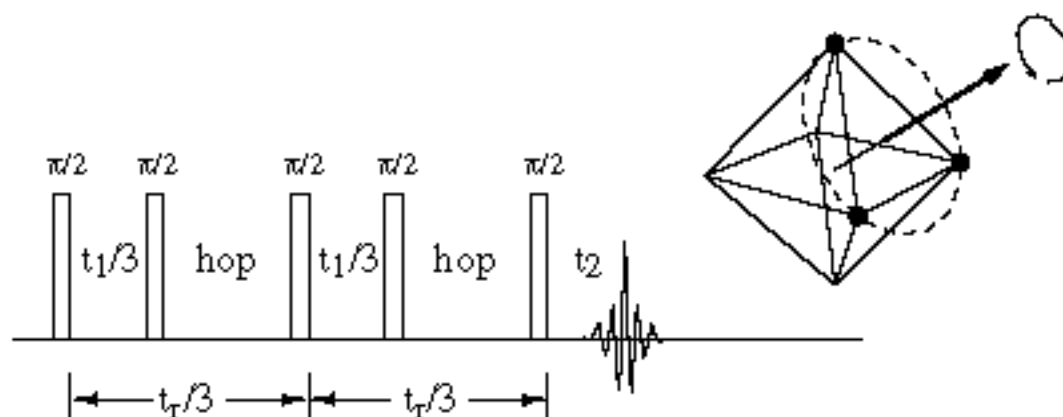


Figure 6.6 Magic-Angle Turning Experiment. Pulses and hops are indicated schematically. The phase cycle is the same as the MAH experiment (see table 6.1). Each hop is performed by allowing the rotor to shift by 120° degrees. As in the previous experiment, each $t_1/3$ period is spent with the magnetization at a different vertex of the octahedron, giving a shifting isotropic echo.

The theory for this experiment is identical in the limit of very slow spinning ($t_1 \ll \tau_r$). In the intermediate case, where t_1 represents is a significant portion of τ_r (the period of the sample rotation), the theory must be written slightly differently. Now instead of the sum of three evolution periods, the frequency expression will be the sum of three integrals of the time-dependent frequencies. The expression for the NMR frequency of a sample rotating about an axis oriented at β^{rot} with respect to the magnetic field as a function of both crystallite orientation $(\alpha^{CS}, \beta^{CS}, \gamma^{CS})$ and time is given below.

$$\omega_{CSA}(t) = \delta_{iso,cs}\omega_l + \sqrt{\frac{2}{3}}\delta^{CS}\omega_l R_{20}^{CS}(t)$$

$$R_{20}^{CS}(t) = \sum_{m=-2}^2 e^{-im(\omega_r t + \phi_r)} d_{m0}^{(2)}(\beta^{rot}) A_{2m}^{CS} \quad (6.27)$$

In this expression the A_{2m}^{CS} term is identical to the A_{2m}^{CS} in equations 2.35 and 6.20. Now the net evolution following the MAT pulse sequence will be the sum of three integrals given below.

$$\phi^{MAT}[t_1] = \delta_{iso,cs}\omega_l t_1 + \sqrt{\frac{2}{3}}\delta^{CS}\omega_l \left[\int_0^{\frac{t_1}{3}} R_{20}^{CS}(t) dt + \frac{\tau_r + t_1}{3} R_{20}^{CS}(t) dt + \frac{2\tau_r + t_1}{2\tau_r} R_{20}^{CS}(t) dt \right] \quad (6.28)$$

Again, the first term is the isotropic chemical shift and the second corresponds to the anisotropic parts. The integrals themselves are over sums which can be separated into a larger sum of integrals. The time-independent part is proportional to the second-order Legendre polynomial of $\cos\beta^{rot}$. This is analytically zero, since we have chosen β^{rot} to be the magic-angle, 54.74° , which means the sum in equation 6.29 will contain no $m = 0$ terms. Each of the integrals may be performed analytically and regrouped below.

$$\phi^{MAT}[t_1] = \delta_{iso,cs}\omega_l t_1 + \sqrt{\frac{2}{3}}\delta^{CS}\omega_l \sum_{m=-2}^2 \frac{e^{-im\phi_r}}{im\omega_r} d_{m0}^{(2)}(\beta^{rot}) A_{2m}^{CS} \left[\exp\left(\frac{-im\omega_r t_1}{3}\right) \exp(0) - \exp(0) + \exp\left(\frac{-im\omega_r t_1}{3}\right) \exp\left(\frac{-im\omega_r \tau_r}{3}\right) - \exp\left(\frac{-im\omega_r \tau_r}{3}\right) + \exp\left(\frac{-im\omega_r t_1}{3}\right) \exp\left(\frac{-im\omega_r 2\tau_r}{3}\right) - \exp\left(\frac{-im\omega_r 2\tau_r}{3}\right) \right] \quad (6.29)$$

These may be further simplified since $\omega_r \tau_r = 2\pi$.

$$\phi^{MAT}[t_1] = \delta_{iso,cs}\omega_l t_1 + \sqrt{\frac{2}{3}}\delta^{CS}\omega_l \sum_{m=-2}^2 \frac{e^{-im\phi_r}}{im\omega_r} d_{m0}^{(2)}(\beta^{rot}) A_{2m}^{CS} \left[\exp\left(\frac{-im\omega_r t_1}{3}\right) C_m - C_m \right] \quad (6.30)$$

The C_m in this expression is identical to that in 6.24. Using the fact that C_m is zero, yields the same frequency expression as in equation 6.26.

$$\begin{aligned}\phi^{MAT}[t_1] &= \delta_{iso,cs}\omega_1 t_1 \\ S(t_1) &= e^{-i\phi^{MAT}[t_1]} = e^{-i\delta_{iso,cs}\omega_1 t_1}\end{aligned}\tag{6.31}$$

Therefore an anisotropic echo in t_2 will appear at a time $t_1/3$ following the last pulse in the MAT sequence which has evolved in t_1 with an isotropic frequency. In both the MAH and MAT experiments, however, signal is lost due to the z-filters. In fact, if the z-filters could be eliminated, a factor of 2 signal-to-noise could be recovered.

A possible alternative to the MAH and MAT sequences is the MAT⁵⁶ with π pulses (MAT-180) sequence which is shown in figure 6.7.

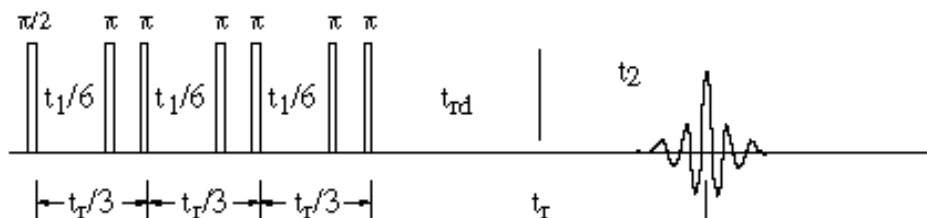


Figure 6.7 Magic-Angle Turning Experiment with Pulses. Pulses are indicated schematically. The phase cycle is given in the text below. In this experiment, no storage pulses are used while rotor shifts by 120° . Each of the $t_1/6$ periods is spent at a different vertex of the octahedron, giving a shifting isotropic echo.

In this experiment, the density matrix is never stored with z-filters. However, now the sequence has been made into a constant time experiment (as t_1 is varied, the MAT isotropic echo will always appear at a point t_r after the last π pulse) which introduces certain other problems which I will discuss later. The phase cycle needed to implement this experiment is quite simple, assuming the π pulses are accurate. Only the first pulse is cycled through four phases and the receiver phase is set equal to this phase (just as in a standard one pulse experiment with cyclops phase cycling.) To show mathematically why this experiment works, we use the same approach as earlier. The phase is expressed below in equation 6.32.

$$\begin{aligned}
\phi^{MAT-180}[t_r] &= \int_0^{\frac{t_1}{6}} \omega_{CSA}(t) dt - \int_{\frac{t_1}{6}}^{\frac{t_r}{3}} \omega_{CSA}(t) dt \\
&+ \int_{\frac{t_r}{3}}^{\frac{t_1}{6} + \frac{t_r}{3}} \omega_{CSA}(t) dt - \int_{\frac{t_1}{6} + \frac{t_r}{3}}^{\frac{2t_r}{3}} \omega_{CSA}(t) dt \\
&+ \int_{\frac{t_1}{6} + \frac{2t_r}{3}}^{\frac{t_r}{6} + \frac{2t_r}{3}} \omega_{CSA}(t) dt - \int_{\frac{t_1}{6} + \frac{2t_r}{3}}^{\frac{t_r}{6} + \frac{2t_r}{3}} \omega_{CSA}(t) dt + \int_{\frac{t_r}{6} + \frac{2t_r}{3}}^{\frac{2t_r}{3}} \omega_{CSA}(t) dt
\end{aligned} \tag{6.32}$$

The integral from τ_r to $2\tau_r$ in this sum may be divided into six integrals with the same limits as the corresponding terms in 6.32 and since $\omega_{CSA}(t) = \omega_{CSA}(t + t_r)$, the negative terms will cancel terms from the expansion of the last integral. The expression for the CSA frequency may be substituted in 6.32 and the time-independent terms removed from the integrals as in 6.27 and 6.28.

$$\begin{aligned}
\phi^{MAT-180}[t_r] &= \delta_{iso,cs} \omega_l t_1 + \sqrt{\frac{2}{3}} \delta^{CS} \omega_l \int_0^{\frac{t_1}{6}} R_{20}^{CS}(t) dt + 2 \int_{\frac{\tau_r}{3}}^{\frac{2\tau_r + t_1}{6}} R_{20}^{CS}(t) dt \\
&+ 2 \int_{\frac{2\tau_r}{3}}^{\frac{4\tau_r + t_1}{6}} R_{20}^{CS}(t) dt
\end{aligned} \tag{6.33}$$

This integration may be performed as earlier, yielding the same phase as in the MAH and MAT experiments.

$$\begin{aligned}
\phi^{MAT-180}[t_r] &= \delta_{iso,cs} \omega_l t_1 \\
S(t_1) &= e^{-i\phi^{MAT-180}[t_r]} = e^{-i\delta_{iso,cs} \omega_l t_1}
\end{aligned} \tag{6.34}$$

This shows that all three experiments give the identical result. The difference between the MAT-180 and the MAT experiment lies in the sensitivity and resolution. In the MAT experiment, the resolution is improved by taking more t_1 points with a corresponding longer total $2t_r$ time. The sensitivity, however, is a full factor 2 worse than the MAT-180 sequence (meaning a factor of 4 more scans are needed). In the case of MAT-180, to enhance the resolution, the rotor must be slowed down (since the longest available t_1 point is for $t_1 = 2t_r$). Since this is a constant-time experiment, there will be more transverse (T_2) relaxation for the same t_1 point at slower speeds than at faster speeds since each t_1 point has identical $2t_r$ transverse relaxation scaling the overall intensity. At some point,

in attempting to gain further resolution in a MAT-180 experiment, the relaxation intensity loss will become larger than the factor of 2 loss due to z-filters in the MAT or MAH experiments. At this point, it is more profitable to use the MAH or MAT experiment in favor of the MAT-180 sequence. Finally, since the MAT-180 sequence is constant time, there should be no net homonuclear dipolar contribution to a spin-1/2 isotropic spectrum (as is the case for the MAT sequence). In addition, both the MAT and MAT-180 may be performed over more than one or two rotor cycles.

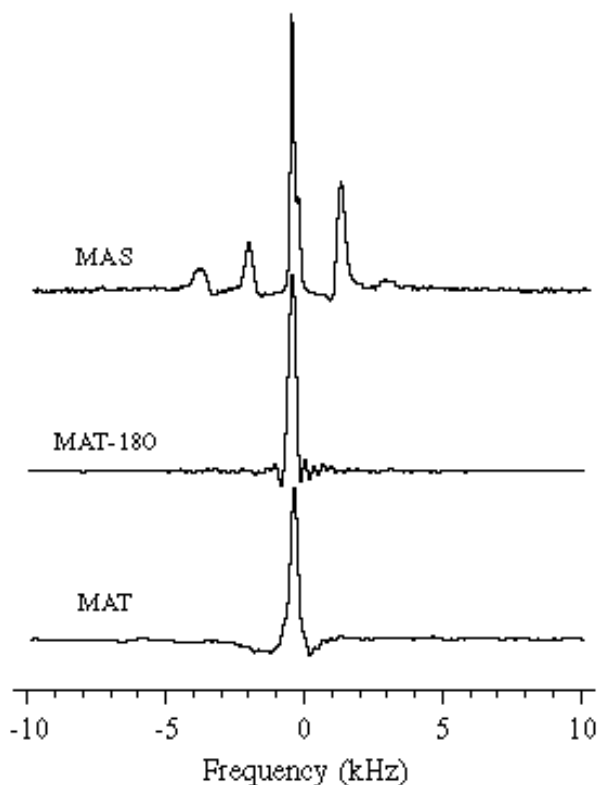


Figure 6.8 MAS, MAT and MAT-180 Spectra of $^{207}\text{PbNO}_3$. All of these spectra represent 64 points in t_1 zero filled to 512. The dwell times were $50 \mu\text{s}$ and the 90° pulse widths were $12 \mu\text{s}$.

In the case of MAT, any number of rotor cycles may be used which is not a multiple of three, while for MAT-180, any even number of rotor cycles which is not a multiple of three may be used. (If the number of rotor cycles is a multiple of three, each of the three evolution periods will have identical starting phase and no averaging will result.) Figure 6.8 shows the MAS, MAT and MAT-180 spectra of $^{207}\text{PbNO}_3$. Notice, in this case, the

signal-to-noise ratio of the MAT-180 spectrum is slightly better than in the MAT spectrum, since the $2 t_r$ time was chosen to be relatively short. This has the adverse effect of adding truncation artifacts to the spectrum in the form of "sinc" wiggles.

Dynamic-Angle Hopping (DAH)

In the previous section on magic-angle hopping methods were discussed which produce sideband-free isotropic spectra. In the case of spin-1/2 nuclei, a number of techniques are already available which produce sideband free evolution.¹¹⁵⁻¹²² The application of these methods to central transitions of quadrupolar nuclei is somewhat limited, especially in the case where sidebands overlap centerband features. The ideas of MAH, however, may be applied equally well to the quadrupolar problem (DAH).^{56,113} In the quadrupolar case the integrals of equation 6.29 will involve a sum from $m = -4$ to $+4$. The additional $m = \pm 3$ and ± 4 terms will cause the simple MAH and MAT experiments to fail, since the value of $C_m = 0$ for $m = \pm 3$ and ± 4 . To average these as well, five different evolution windows are needed (in the case of hopping about the magic-angle). In this case, the expression for C_m is given below (which is zero for all $m < 5$).

$$C_m = 1 + e^{-\frac{2im\pi}{5}} + e^{-\frac{4im\pi}{5}} + e^{-\frac{6im\pi}{5}} + e^{-\frac{8im\pi}{5}} \quad (6.35)$$

This is still not sufficient to produce isotropic spectra, since five hops about the magic-angle will *only* give a sideband free MAS spectrum (not altogether useless). To isotropically average a quadrupolar central transition, it has been shown that multiple spinning axes are required.^{16,42,43,55,113} The solution to the problem is to use two DAS angles and use five evolution periods at each angle to cancel the time dependent terms. This is a total of 10 evolution periods, needing a minimum of 9 z-filters to store magnetization during hops. This is almost certainly an unacceptable number and therefore a better solution is to choose the DAS angle pair which simplifies the problem. The $k = 5$ angle pair of 63.43° and 0.00° is the best angle pair for this sort of experiment, since at 0.00° there are

no time-dependent terms. Thus, to do the DAH experiment, we merely spin slowly about the angle 63.43° with respect to the magnetic field. Under these conditions we use 90° pulses to store the evolution between the five 72° jumps. Following these five evolution periods, the magnetization is stored as the spinning axis is realigned to 0.00° and evolution is allowed to proceed again. This experiment still needs a total of 5 z-filters for magnetization storage, but this represents a factor of 4 improvement in signal-to-noise over the 9 z-filter experiment proposed earlier (unfortunately it is still a factor of 4 worse than in a conventional DAS experiment).

The phase cycle needed to implement this DAH experiment is quite long, since a large number of pulses are involved in the sequence. The schematic pulse sequence and the equation which describes the relationship between the eleven 90° pulses and the receiver phases are given below. The time t_{72° indicates the time needed to allow the rotor to rotate 72° and the time t_{hop} indicates the time needed to reorient the spinning axis from 63.43° to 0.00° .

$$90^\circ - \frac{t_1}{6} - 90^\circ - t_{72^\circ} - 90^\circ - \frac{t_1}{6} - 90^\circ - t_{72^\circ} - 90^\circ - \frac{t_1}{6} - 90^\circ - t_{72^\circ} - 90^\circ - \frac{t_1}{6} - 90^\circ - t_{hop} - 90^\circ - \frac{t_1}{6} - t_2 \quad (6.36)$$

$$-\phi_1 + \phi_2 - \phi_3 + \phi_4 - \phi_5 + \phi_6 - \phi_7 + \phi_8 - \phi_9 + \phi_{10} - \phi_{11} = -\phi_R$$

In this experiment, the coherence alternates between -1 (during the $t_1/6$ evolution periods) and 0 (during the t_{72° z-filter storage periods). To achieve this, the first pulse should be cycled through four phases to choose the -1 coherence transfer and the second will be uncycled, assuming that the 72° hopping period will be sufficiently long that all transverse magnetization will decay away. This, in theory, should be continued for each of the next 8 pulse pairs. The last pulse may be left uncycled, since the receiver quadrature will select the -1 pathway. This is a total of 4^5 , or 1024, steps in the phase cycle. In many situations, this is too many steps to do a phase cycle over for a spectrometer (i.e. the BrukerTM AM-400) or more scans than is possible in a two-dimensional experiment due to

long relaxation times (remember that the isotropic DAH signal must be collected point by point in t_1 just as in DAS). One solution is to use only cycles of pulse phases of three rather than four. This will still choose only a $\Delta\mathbf{p} = -1$, however this may be difficult to implement on some spectrometers. Also, it still requires a total 3^5 , or 243, steps which is over a factor of four fewer scans. In the case where fewer scans are desired, it is necessary to choose fewer pulses to cycle. It is probably best to cycle pulses closer to the beginning of the sequence, thereby guaranteeing the coherence pathway for most of the early steps. This can lead to experimental artifacts. Ideally, we should cycle the other pulses (except the last) through two steps to guarantee no transverse components during z-filters. This will expand the phase cycle again by a factor of 2^5 (a total factor of 32).

A final note about the sequence is that the five angles at 63.43° and one at 0.00° are equivalent to the static magnetic field being rotated to point through the vertices of an icosahedron (which has the symmetry needed to average first and second order interactions) in the PAS coordinate system.

A second implementation of the DAH experiment is to use 180° pulses (DAH-180), just as in the MAT-180 sequence. Instead of storing the magnetization with z-filters, we can instead apply rotor synchronized 180° pulses in the following sequence, where the time variables have the same meaning as before.

$$\begin{aligned}
&90^\circ - t_r - \frac{t_1}{12} - 180^\circ - t_{72^\circ} - 180^\circ - \frac{t_1}{12} - 180^\circ - t_{72^\circ} - 180^\circ - \frac{t_1}{12} - 180^\circ - t_{72^\circ} - 180^\circ \\
&\quad - \frac{t_1}{12} - 180^\circ - t_{72^\circ} - 180^\circ - \frac{t_1}{12} - 180^\circ - t_{72^\circ} - 90^\circ - t_{hop} - 90^\circ - \frac{t_1}{6} - t_2
\end{aligned} \tag{6.37}$$

$$\begin{aligned}
&-\phi_1 + 2\phi_2 - 2\phi_3 + 2\phi_4 - 2\phi_5 + 2\phi_6 - \\
&\quad 2\phi_7 + 2\phi_8 - 2\phi_9 + 2\phi_{10} - \phi_{11} - \phi_{12} = -\phi_R
\end{aligned}$$

The phase cycle needed to implement DAH-180 is much simpler than for DAH, assuming the 180° pulses are accurate and lead to only a ± 2 coherence transfer. In this case, only the first pulse needs to be cycled through four phases and the eleventh through two (just as in the original DAS experiment). In fact, the sequence is identical to the original

DAS experiment with the addition of nine 180° pulses. These may be ignored in this case for phase cycling purposes. Any of the pure-phase modifications discussed in chapter 4 may be used here to enhance the overall signal-to-noise in the two-dimensional spectrum (if the we are interested in an isotropic/anisotropic correlation spectrum). Again, both the DAH and DAH-180 cycles may be implemented over more than two rotor cycles, just as in the case of MAT and MAT-180. Since the frequency expansion has sines and cosines up to $4 \omega_r$, the number of evolution periods must always be larger than this (we choose 5), and the number of rotor periods the experiment is performed over must not be a multiple of the number of evolution periods (in this case 5). The mathematics needed to prove these features for the DAH and DAH-180 are identical to the case of MAT and MAT-180. These types of experiments have recently been discussed by Gann *et al.*⁵⁶ and Alderman *et al.*¹²³ and I would direct the interested reader to these papers for additional information.

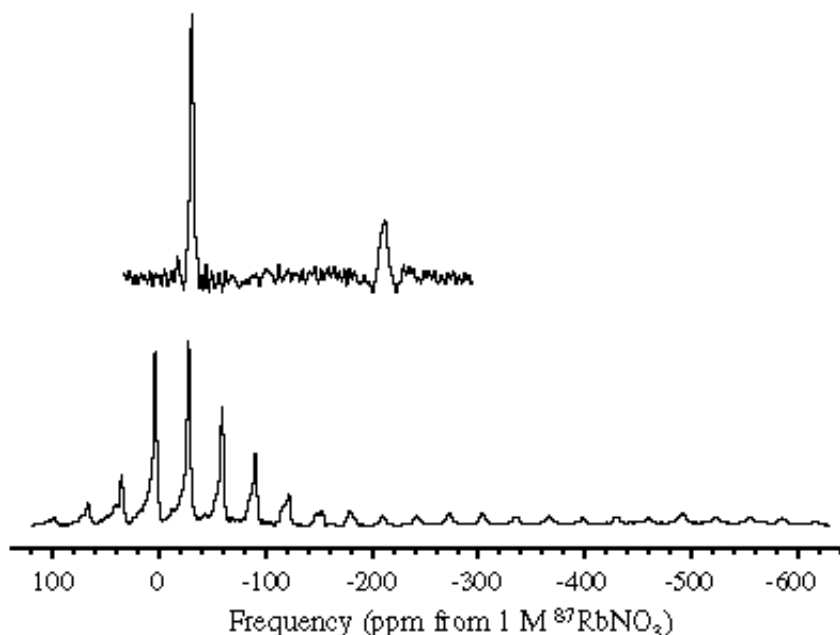


Figure 6.9 DAS and DAH 1D spectra of $^{87}\text{Rb}_2\text{CrO}_4$. The upper DAH spectrum shows no spinning sidebands and the isotropic peaks are easily identified, while in the lower DAS spectrum the broad site with an isotropic shift at -201 ppm breaks into a large number of sidebands. A second spinning speed would be needed to identify this as the isotropic site using this method.

Figure 6.9 shows the DAS and DAH spectra for rubidium chromate ($^{87}\text{Rb}_2\text{CrO}_4$) taken at 9.4 T which has two sites. Both sites appear in the DAS spectrum, however the broad site with an isotropic shift at -201 ppm is greatly reduced in intensity due to the large number of spinning sidebands. Even the more intense peak at -27 ppm has at least six spinning sidebands in this spectrum. The appearance of the isotropic peak at -201 ppm in the DAH spectrum shows the power of the DAH experiment. This peak is much more intense than the same peak in the DAS spectrum. This peak, unfortunately, is broadened more than the peak at -27 ppm, thereby making the intensity seem much less than the expected 1:1 ratio. This is probably due to angle errors during the 72° hops while spinning at 63.43° which result from fluctuations in the spinning rate. Finally, because of the large number of z-filters, the DAH experiment required over 20 times the number of scans and therefore 20 times the overall experiment time as the comparable DAS experiment. This factor negates much of the benefit of DAH, since the same information may be attained with just two DAS experiments in a tenth the time.

In figure 6.10 we see the DAS and DAH-180 spectra for rubidium sulfate ($^{87}\text{Rb}_2\text{SO}_4$) at 9.4 T which also has two sites. Both sites appear in both spectra. However, in the DAH-180 spectrum, there are no spinning sidebands to complicate the interpretation. Also, the intensities of the two peaks should reflect the population at the two sites (which is 1:1 in this case). For the DAS spectrum, intensity measurement necessitates integration of a large number of spinning sidebands (some of which overlap). If we compare only the heights of the isotropic centerbands, we arrive at a ratio of 2.8 (-25 ppm site) to 8.5 (29 ppm site). This 1:3 ratio is much less than expected from the crystal structure. Taking the heights of each sideband as the integral and adding up the intensity for each of the sidebands in the DAS spectrum, yields intensities of 9.2 (-25 ppm site) and 10.1 (29 ppm site). These are, as expected, quite close to the 1:1 ratio, however, in samples with multiple sites, integration of sideband intensity may be impos-

sible. For the DAH-180 spectrum, we may easily integrate each of the two peaks (2.62 and 2.34 intensities respectively) and get the correct 1:1 ratio.

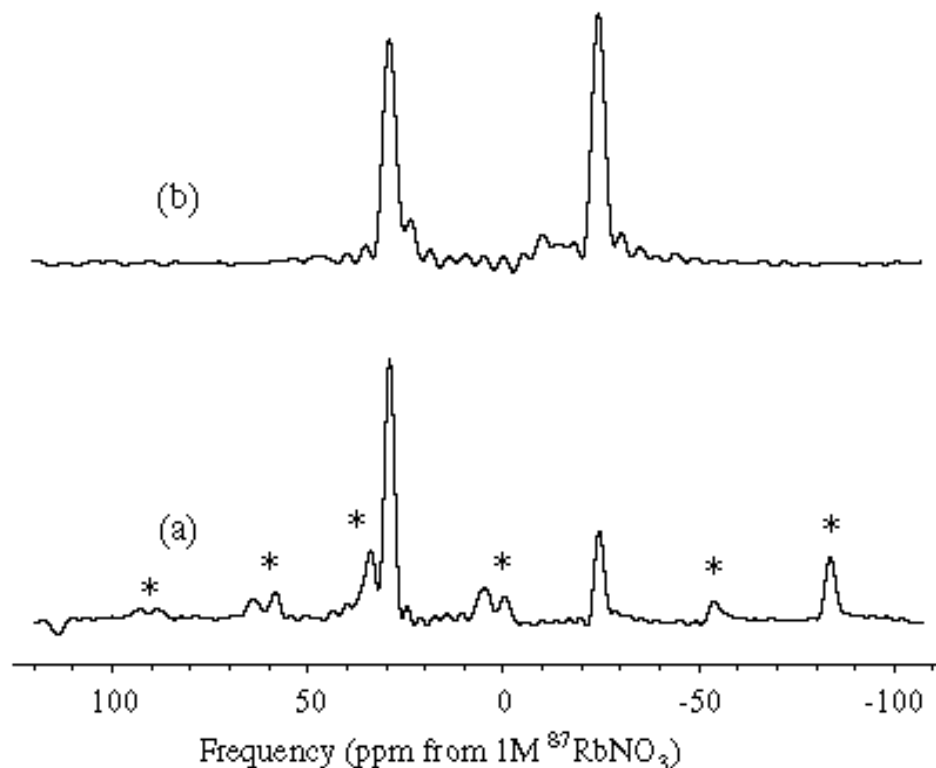


Figure 6.10 DAS and DAH-180 1D spectra of $^{87}\text{Rb}_2\text{SO}_4$; Spectrum (a) shows the 9.4T DAS spectrum of $^{87}\text{Rb}_2\text{SO}_4$ taken at a spinning rate of 5 kHz and with the SEDAS pulse sequence. Spinning sidebands are indicated with asterisks. Spectrum (b) shows the 9.4T DAH-180 spectrum of the same compound taken with the 9 pulse sequence applied over 8 rotor cycles at 2.4 kHz.

As was mentioned earlier for the MAT-180 sequence, constant-time experiments may sometimes present sensitivity problems when additional resolution is needed. The DAH-180 sequence is partially a constant-time experiment since 5/6 of the t_1 evolution occurs under constant time conditions. Therefore, as can be seen in figure 6.10, we often get truncation artifacts in DAH-180 spectra. These sequences, however, show great promise for studying systems where an inhomogeneous distribution of isotropic shifts exists, for example in an amorphous solid such as a glasse (see chapter 8). In these cases, the distribution of isotopic shifts leads to a rapid dephasing in t_1 (in fact, much more rapid than the intrinsic T_2 linewidth would suggest). This means that many fewer point

are required in t_1 before the signal disappears. Therefore a constant time experiment such as DAH-180 is uniquely well suited for the study of these systems, just as pulse sequences such as HyperSEDAS are best suited for giving high-sensitivity pure-phase two-dimensional spectra. Combining these two ideas should greatly improve the overall quality of isotropic/anisotropic correlation spectra in amorphous solids.